



Article

Effects of the Second Anodization Parameters on the Hydrophobicity and Anti-Icing Properties of Al Surface with Composite Nanopore Structure

Bo Li ^{1,2}, Jie Bai ^{1,2}, Liuqing Yang ^{1,2}, Lusong Zhang ^{1,2}, Xu Dai ³, Cheng Zhang ⁴ , Xujiang Hua ⁴, Tao Zhu ⁴, Huiying Xiang ⁴, Ruijin Liao ³ and Yuan Yuan ^{4,*} 

- ¹ Institute of Electric Power Science of Guizhou Power Grid Co., Ltd., Guiyang 550002, China; gzgy1b2207@163.com (B.L.); bai_jie25@163.com (J.B.); yanglq0718@163.com (L.Y.); 13984790560@139.com (L.Z.)
- ² China Southern Power Grid Laboratory of Anti-Icing and Disaster Reduction, Liupanshui 553002, China
- ³ State Key Laboratory of Power Transmission Equipment & System Security and New Technology, Chongqing University, Chongqing 400044, China; xudai@cqu.edu.cn (X.D.); rjliao@cqu.edu.cn (R.L.)
- ⁴ School of Materials Science and Engineering, Chongqing University, Chongqing 400030, China; 20163014@cqu.edu.cn (C.Z.); 20230901040@stu.cqu.edu.cn (X.H.); davezhu@cqu.edu.cn (T.Z.); 20200901052@cqu.edu.cn (H.X.)
- * Correspondence: yuany@cqu.edu.cn

Abstract: Icing on transmission lines often causes potential electric damage in power systems. Superhydrophobic anodized Al conductors have been proposed to have good anti-icing properties. In this study, superhydrophobic anodized Al conductors with composite nanopore structures were prepared by a two-step anodization. The microstructure, hydrophobicity, and anti-icing properties of composite nanopore structures were compared and studied. The optimal preparation parameter was determined as a current density of 0.04375 A/cm² and anodization time of 15 min. Compared with the bare substrate, the optimal anodized Al surface of the composite nanopore structures show excellent hydrophobic and anti-icing properties, including a contact angle of 173°, a contact angle hysteresis of 0.122°, an ice adhesion strength of 0.71 kPa, and a glaze icing weight of 0.1 g after the 8 h. Therefore, the prepared anodized Al surface of composite nanopore structures with good anti-icing properties has profound application potential for overhead transmission lines.

Keywords: transmission line; superhydrophobic; anti-icing; two-step anodization; composite nanopores; glaze icing



Citation: Li, B.; Bai, J.; Yang, L.; Zhang, L.; Dai, X.; Zhang, C.; Hua, X.; Zhu, T.; Xiang, H.; Liao, R.; et al. Effects of the Second Anodization Parameters on the Hydrophobicity and Anti-Icing Properties of Al Surface with Composite Nanopore Structure. *Coatings* **2023**, *13*, 1859. <https://doi.org/10.3390/coatings13111859>

Academic Editor: Alessandro Latini

Received: 21 September 2023

Revised: 13 October 2023

Accepted: 23 October 2023

Published: 29 October 2023



Copyright: © 2023 by the authors. Licensee MDPI, Basel, Switzerland. This article is an open access article distributed under the terms and conditions of the Creative Commons Attribution (CC BY) license (<https://creativecommons.org/licenses/by/4.0/>).

1. Introduction

Icing disasters on transmission lines will seriously threaten the safe operation of the power system. Continuous icing on lines will cause line galloping, disconnection, tower collapse, etc., which can finally result in a power interruption [1,2]. As was widely reported in 2008, the major ice and snow disaster in southern China caused serious damage to the power grids of 17 provinces, with direct economic damage of nearly 100 billion CNY [3,4].

At present, the practical icing prevention measures are mainly de-icing technology and meteorological monitoring. As the main de-icing method, although high-current ice melting equipment have a high de-icing efficiency, their main defects are the fact that they have expensive operation and maintenance costs [5]. Meteorological monitoring is limited in its consistency with actual icing [6]. Therefore, the current anti-icing ability of transmission lines in extreme ice and snow climates is still insufficient [3]; hence, it is extremely urgent and necessary to further develop auxiliary and reliable de-icing and anti-icing technologies.

Surface treatment is a simple and effective protection method for metals [7,8]. Based on bionic technology, a superhydrophobic coating with good hydrophobicity can reduce water

droplet adhesion, decrease the ice adhesion strength, and delay the icing time, which is expected to achieve better anti-icing protection of transmission lines [9]. Superhydrophobicity is not completely equivalent to the anti-icing performance, and the low ice adhesion of the superhydrophobic surface is significant for the rapid de-icing of overhead transmission lines [1,10]. Therefore, it is important to study and optimize the anti-icing performance of the superhydrophobic surface. Zhang et al. proposed a spraying technology to realize the hydrophobicity and anti-icing properties of Al conductors [11]. However, the heat caused during the power transmission and the strong ultraviolet radiation in the high-altitude environment will lead to the rapid aging of organic coatings, which is a potential defect of spraying technology [1]. Normally, anodic oxidation is an electrochemical treatment for metal surfaces. This technique adopts the dissolution reaction of the electrolyte under the electric field, in which the valve metal is the anode [10]. This treatment can lead to the formation of a dense and stable ceramic oxide film with a specific structure to improve the durability [1]. Liu et al. have reported a durable anti-icing superhydrophobic anodic alumina surface [1]. Xiang et al. also confirmed the anti-icing performance of anodized aluminum strands [1,12]. Therefore, further considering the anodic oxidation method to achieve precise control of the nanopore's structure can achieve the preparation of good anti-icing Al surface for complex aluminum strands. Moreover, the structural design of an anodized nanopore structure has been the focus of many scholars. The reported structural designs include a dendritic shape [10], bottle type [13], textured dimples [14], etc. These designed nanopore structures, prepared by optimized anodization, can enable the anodized film to achieve multiple functions [15,16], including improving corrosion protection [13], expanding the lubricant capacity [14], and inhibiting the consumption of modified solvents and lubricants [10]. Therefore, the preparation of composite nanopore structures by two anodization processes can theoretically improve the anti-icing performance of traditional anodized pore structures.

Among all types of icing on transmission conductors, glaze icing could be seen as the most serious icing disaster that threatens lines and towers. Glaze icing is a phenomenon that occurs in a climate including slight cold, strong wind, rain with large diameters of water droplets, and an intersection of strong warm and cold air [1]. However, limited by experimental conditions, there are fewer studies on the anti-icing protection of conductors against glaze icing [1,10]; more attention is paid to frost and condensation in indoor rooms, and ice and snow in outer environments [11,17,18]. Therefore, this study is also focused on stimulated glaze icing on conductors in the laboratory.

In this study, a two-step anodizing method was used to successfully prepare a composite nanopore structure on Al conductors by adjusting the anodizing parameters (current density and anodized time). The microstructure, hydrophobicity, and anti-icing properties of the composite nanopore structures were compared and studied. The application prospects of composite nanopore structures prepared by a two-step anodizing technology in transmission Al lines were evaluated and determined.

2. Experiment Setup

2.1. Preparation of Anti-Icing Composite Nanopore Structure

In this study, the raw Al plates (1060) are the same type as Al strands of Aluminum Conductors Steel-Reinforced (ACSR) cable with a size of 20 mm × 20 mm × 1 mm. Before the anodization process, all bare specimens were soaked in a 1 mol/L sodium hydroxide solution for 5 min to remove grease and oxide film from the surface of the Al sheet. After ultrasonic cleaning with deionized water, all specimens were prepared for anodization.

In Figure 1a, the DC stabilized power supply (WYJ-110A) outputs twice the current densities on the bare Al specimens in a 0.3 mol/L phosphoric acid solution and a 0.15 mol/L oxalic acid solution, respectively. The temperature of the reaction process is controlled by a magnetic stirrer and water chiller (CZ3457-5HP). Here, all Al plates were used as the anode, while the 305 stainless steel sheets were used as the cathode. The first step of anodization puts forward the 0.0875 A/cm² on specimens for 10 min, which was referred

to in previous studies. After, the second step of anodization outputs different current densities (0.01875 A/cm^2 , 0.04375 A/cm^2 , 0.06875 A/cm^2) for 10 and 15 min. These anodized specimens were named 0.01875 A 10 min, 0.01875 A 15 min, 0.04375 A 10 min, 0.04375 A 15 min, 0.06875 A 10 min, and 0.06875 A 15 min, respectively. After the two anodization processes, all anodized specimens were modified with 3 wt. % heptafluorodecyltrimethoxysilane (FAS-17) ethanol solution under a vacuum environment of -0.1 MPa for 12 h, then dried in an oven of $90 \text{ }^\circ\text{C}$ for 30 min to achieve the anti-icing Al surface with a composite nanopore structure.

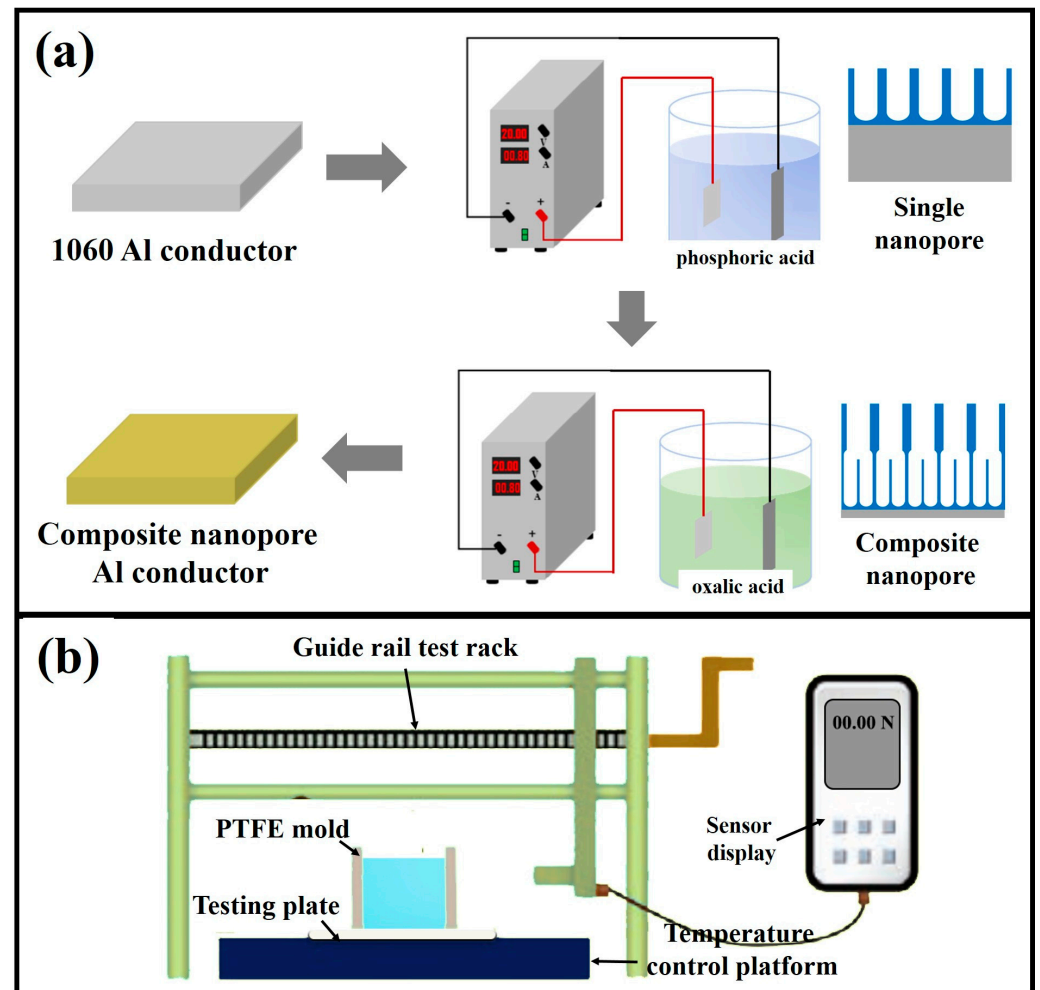


Figure 1. Experimental platforms: (a) anodization equipment; (b) icing experimental chamber.

2.2. Experimental Setup

Microstructure and elemental analysis of samples were characterized by scanning electron microscopy (SEM, Zeiss Auriga, Jena, Germany) with an energy dispersive spectroscopy (EDS) probe equipped with the SEM equipment. The voltage parameter during SEM testing was 3–5 kV, and the voltage parameter during energy spectrum analysis was 20 kV. The surface roughness of the sample was measured using a confocal laser scanning microscope (LM, LEXT OLS4000, Olympus, Tokyo, Japan). The contact angle and contact angle hysteresis were measured by a CA testing meter (SDC-100, SINDIN, Dongguan, China). The measurement environment was the room temperature ($25 \text{ }^\circ\text{C}$) and room humidity (50.2% RH). A high-speed camera (Revealer, M220, Fuhuang AgileDevice Ltd., Hefei, China) with a real-time capture system was adopted to capture the motion behavior of falling water droplets on different surfaces at $-3 \text{ }^\circ\text{C}$.

In Figure 1b, ice adhesion tests were to put the PTFE cylinder mold (with a diameter of 8 mm) full of water on the samples, while the samples were on the cooling plate at $-3\text{ }^{\circ}\text{C}$ and 50.2% RH for 6 h. The temperature was controlled by a high-precision semiconductor constant temperature experimental platform (LTD1-350, Chongqing, China). Then, the thrust meter was used to push away the iced mold. Ice adhesion was obtained by dividing the thrust indicator by the contact area. In addition, the condensation and frost formation processes of the sample were also conducted on the cooling plate at $-3\text{ }^{\circ}\text{C}$, and the surface frost process was recorded using a camera. For evaluating the glaze icing behaviors, the icing process of specimens was observed in the artificial icing experimental chamber. The falling water droplets had a diameter of about $350\text{ }\mu\text{m}$. The testing temperature, humidity, and wind speed were $-3\text{ }^{\circ}\text{C}$, 80% RH, and 3 m/s. Finally, the anodized sample of optimal anti-icing properties was determined through orthogonal experiments.

3. Results and Discussion

3.1. Morphologies and Micro-Structures

Figure 2 shows SEM images and the corresponding surface roughness of anodized specimens. In Figure 2a–f, when the anodization time is 10 min and the applied current density increases (0.01875 A/cm^2 – 0.06875 A/cm^2), the diameter of the nanopore increases from 230 nm to 280 nm, the porosity increases from 70% to 74%, and the gap ratio (the hole spacing divided by the hole wall) increases from 3.53 to 7.56. When the anodization time is 15 min and the applied current density increases, the surface pore size of the sample increases from 290 nm to 310 nm, the porosity increases from 73% to 77%, and the gap ratio increases from 9.17 to 12.56.

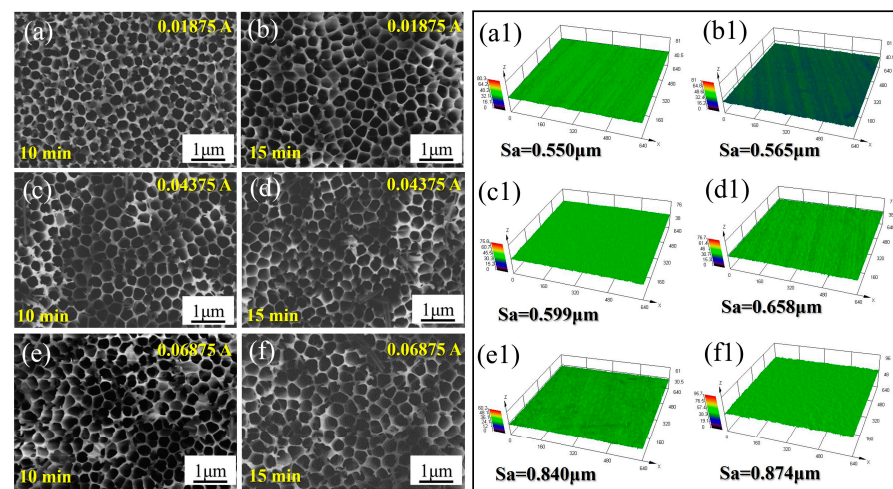


Figure 2. Morphological images and surface roughness of anodized specimens with different electric parameters: (a,a1) 0.01875 A 10 min, (b,b1) 0.01875 A 15 min, (c,c1) 0.04375 A 10 min, (d,d1) 0.06875 A 15 min, (e,e1) 0.06875 A 10 min, and (f,f1) 0.06875 A 15 min.

The 3D morphology and roughness of the samples are shown in Figure 2a1–f1. As the current density and anodization time increase, the dissolution effect gradually enhances and the surface roughness of the sample gradually increases. When the current density is low (0.01875 and 0.04375 A/cm^2), the dissolution effect of oxalic acid is not obvious, and the surface roughness reaches 0.550 and $0.658\text{ }\mu\text{m}$. However, when the current density is 0.06875 A/cm^2 , the surface roughness increases to 0.84 and $0.87\text{ }\mu\text{m}$. This indicates that a higher current density and longer anodization time can cause excessive dissolution and fragmentation of the surface structure and the appearance of micron-level disordered fluctuation [1].

Figure 3 depicts cross-sectional micrographs of all specimens. Obviously, the small pore structure (the first anodization) continues to grow downwards along the basis of the large pore structure (the second anodization) until the Al substrate forms a composite

nanopore structure. Moreover, as the current density and anodization time of the second anodization increase in Figure 3, the thickness of the lower small nanopore structure gradually increases. However, the thickness of the upper large nanopore membrane slightly decreases due to the dissolution effect of the oxalic acid anodization process [1]. When the anodization time is 10 min, the thickness of the lower layer increases from 4.11 μm to 15.30 μm with the increase in current density. When the anodization time is 15 min, the thickness of the small pore size film increases from 5.66 μm to 21.31 μm with the increase in oxidation current density. In all, the formation of a thicker anodized film can be attributed to the stronger passivation effect at a higher power.

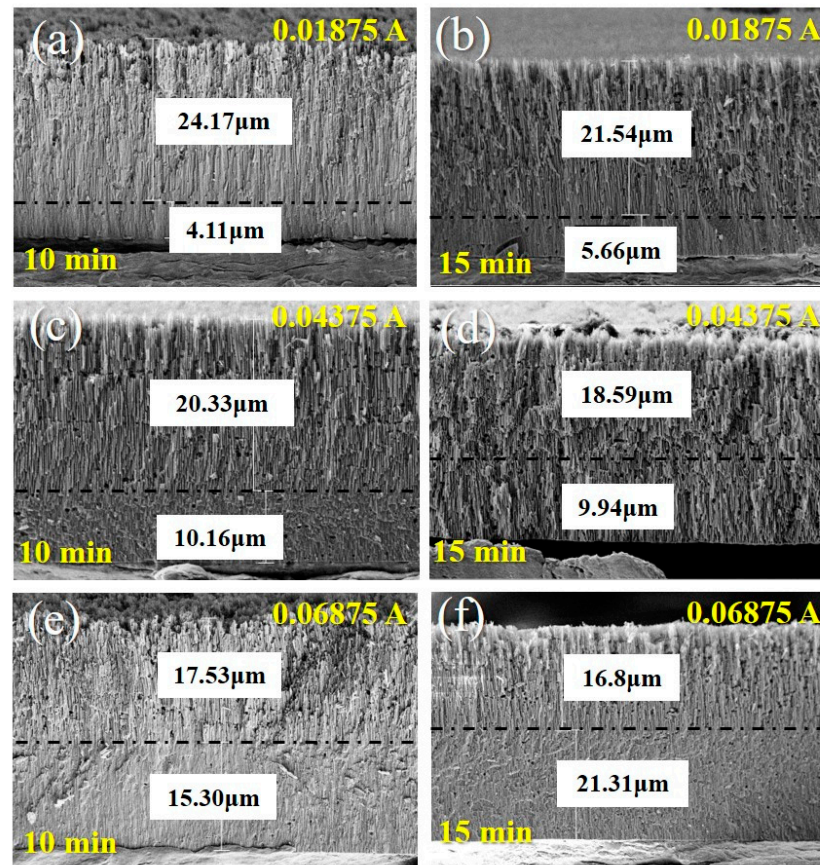


Figure 3. The cross-sectional thickness of specimens: (a) 0.01875 A 10 min, (b) 0.04375 A 15 min, (c) 0.06875 A 10 min, (d) 0.04375 A 15 min, (e) 0.06875 A 10 min, and (f) 0.06875 A 15 min.

3.2. Wettability and Anti-Icing Properties

The surface wettability can be obviously affected by the microstructure and roughness. In Figure 4, the contact angle and contact angle hysteresis of different specimens did not change much. Under different electric parameters, the contact angle of all samples remains above 163° in Figure 4a. When the anodization time is 10 min, the contact angle of the sample surface changes from 163° to 166° to 165° with the increase in current density. The contact angle hysteresis shows a similar value between 4.113° and 2.629° in Figure 4b. Notably, the contact angle of the specimen reaches a peak of 173° when the oxidation time is 15 min, and the current density is $0.04375 \text{ A}/\text{cm}^2$. However, a continued increase in the current density and oxidation time can decrease the contact angle (168°). This can be explained as when the current density of oxalic acid anodization is too high, the surface pore's structure is broken due to excessive dissolution, resulting in an increase in roughness, the appearance of micro-level rough structures, and decreased hydrophobicity [1]. Here, the sample of $0.04375 \text{ A}/\text{cm}^2$ and 15 min shows the best superhydrophobic properties of 173° and 0.30° .

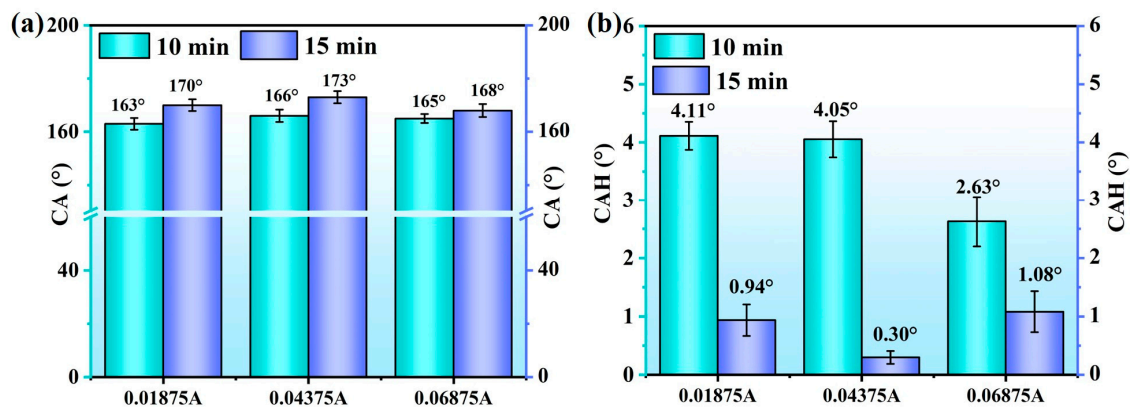


Figure 4. Wettability of different anodized specimens: (a) contact angle; (b) contact angle hysteresis.

Ice adhesion is an important parameter to evaluate the anti-icing property. In Figure 5, it is obvious that the anodized samples have improved the ice adhesion strength of the Al substrate (59.44 kPa). When the anodization time is 10 min, with the increase in current density, the increased porosity and gap ratio of the composite nanopore structure can improve the superhydrophobicity and ice adhesion (17.73 kPa to 2.56 kPa). When the anodization time is 15 min, the ice adhesion of all specimens shows a low level, which is consistent with the above results. The increased current density and anodization time can excessively dissolve the nanopore structure, resulting in the increased roughness of fluctuated structures. Therefore, some water droplets can transit from the Cassie state to the Wenzel state, infiltrate into the surface pore structure and form the interlocking effect, resulting in an increase in ice adhesion strength [18]. In particular, the specimen of 0.04375 A/cm² and 15 min shows the best icephobicity of 0.71 kPa.

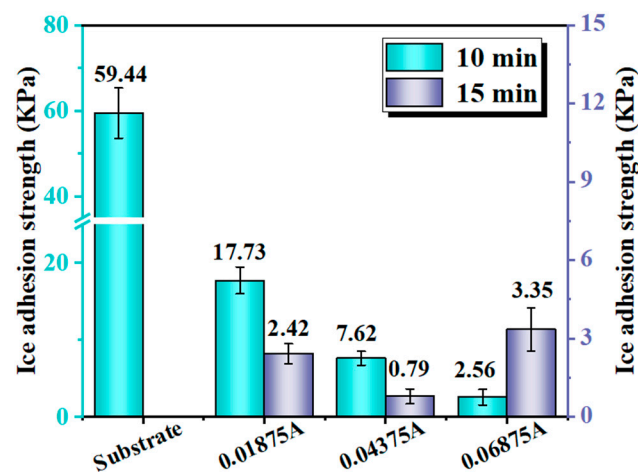


Figure 5. Testing results of ice adhesion strength of bare and anodized specimens.

The frosting behavior is an important indicator to evaluate the anti-icing properties [1]. Figure 6 depicts the frosting process of different anodized specimens. After frosting for 30 min, the surface of 0.04375 A and 15 min shows many spherical condensation water droplets without obvious frost crystal formation. However, surfaces of other parameters are covered by frost film to varying degrees. After 120 min of condensation frosting, the central surface of the 0.04375 A and 15 min specimen still shows few frost crystals with small spherical condensate droplets. In contrast, other specimens can be found in the thick and sparse frosting accumulation. The excellent anti-frosting behavior of specimens (0.04375 A and 15 min) can be attributed to the delayed heat transfer at three-phase interfaces, and the existence of an air cushion, finally leading to prolonged frost formation. The bad

frosting behavior could result from the broken and uneven composite nanopore structure, promoting the uneven nucleation of frost crystals and shortening the complete frosting time.

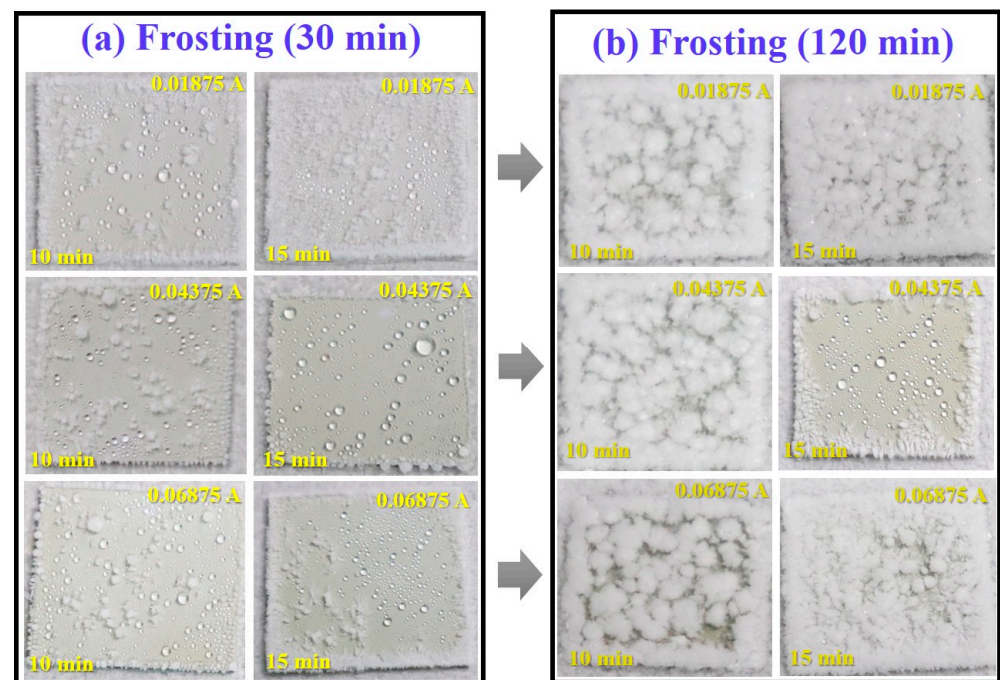


Figure 6. Frosting process of different anodized specimens for prolonged time: (a) 30 min; (b) 120 min.

Based on the above, the anodized sample (0.04375 A and 15 min) of optimal wettability and anti-icing properties can be determined through orthogonal experiments. The anti-icing mechanism of the prepared composite nanopore structure is further studied. In Figure 7, the contact angle of the bare Al surface is 56° , while the contact angle hysteresis is 29.78° . When the substrate was modified with FAS-17, the contact angle increased to 102° and the contact angle hysteresis decreased to 18.89° . For the composite nanopore structure without modification with FAS-17, the water droplets are easily embedded in the micro-nanopores to form a Wenzel state, resulting in a significant decrease in the contact angle of 26° and an increase in the contact angle hysteresis of 43.961° . After the modification in the composite nanopore structure, the large nanopores capture the air to form air cushions between the water droplets and solid surface so that the water droplets are in a Cassie state [1]. The contact angle of the composite nanopore structure can increase to 173° , and the contact angle hysteresis can decrease to 0.122° . Therefore, the modified composite nanopore structure is significant for exhibiting good wettability.

In the environment of overhead transmission lines, glaze icing shows the most harmful influence of all icing due to its significantly high ice density and adhesion. Before simulating glaze icing, glaze icing is initially the process of water droplets hitting the surface. After, spreading, shrinking, and rebounding of the droplets will subsequently occur. In particular, the main parameters of the motion process are the maximum rebound height, contact time, and spreading coefficient, respectively. For the maximum rebound height, this can measure the energy loss of droplets after hitting the surface; contact time is the duration time from hitting to leaving the surface. A shorter contact time shows a shorter heat exchange time, indicating it is less prone to freezing; the spreading coefficient is the ratio of the maximum spreading diameter and the diameter of water droplets before impact (D/D_0), indicating the degree of deformation after the impact. A smaller spreading coefficient can reflect a smaller contact area between the water droplets and the surface, leading to less heat exchange and, thus, harder freezing [1].

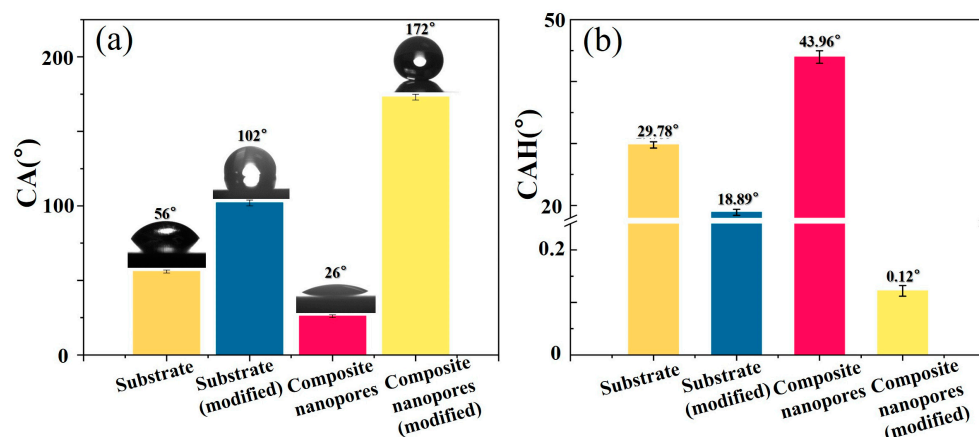


Figure 7. Wettability comparison of bare and anodized specimens of composite nanopores before and after modification: (a) contact angle; (b) contact angle hysteresis.

In Figure 8a–d, all water droplets spread to the maximum area at 2 ms after impacting on various Al surfaces. Moreover, the spreading coefficient of water droplets on the substrate is 4.89, while that of the composite pore aluminum surface is 5.15. After modification, the spreading coefficients of water droplets are reduced to 3.945 and 2.57 in Figure 8c,d due to the decrease in surface energy. After reaching the maximum spreading area, water droplets will gradually shrink on the surfaces. For the substrate and substrate (modified) in Figure 8a,b, the water droplets shrink to a hemisphere of 15 ms and then stay on the surface stably. For the unmodified composite nanopores, the water droplet can easily penetrate the porous structure in a Wenzel state, causing a high resistance to shrinking to a hemisphere shape and adhering to the surface in a spreading shape. In all, substrate, substrate (modified), and composite nanopores cannot have the rebound behavior of droplets due to the large energy loss. However, the modified composite nanopores show obviously different behavior in Figure 8d for the air cushion and low surface energy. For the whole motion behavior of composite nanopores (modified), the impacting water droplet rapidly shrinks into a spherical shape after reaching the maximum spreading area, then rebounds off the surface at 8 ms and rebounds to a maximum height of 16.50 mm at 63 ms. After, the water droplets fall again to a place outside the surface at 108 ms. In particular, the motion data of the water droplet on the modified composite nanopores shows the smallest spreading coefficient during the impact process, shortest contact time, and highest maximum rebound height. This further indicates the decreased energy loss, causing the delayed freezing of water droplets on the surface [1].

Good motion behavior of impacting droplets on the surface cannot completely evaluate the glaze icing behavior due to the lack of a low-temperature environment [1]. The icing weight and icing shape of the anti-icing surface are also important to reflect anti-icing properties [19]. Figure 9a depicts the simulated glaze icing platform, including the artificial glaze ice testing chamber, water spray, and specimens placed at the 45° slope, etc. Under the typical glaze icing conditions of temperature $-3\text{ }^{\circ}\text{C}$, humidity 80% RH, and wind speed 3 m/s, glaze icing tests of different specimens were carried out for 8 h. The icing morphology and weight of the samples are shown in Figure 9b–e and Table 1. Figure 9b,c depicts the severe icing morphologies of the substrate and substrate (modified), reflected in the complete cover of a thick ice layer and long icicles downward at the lower edge of samples. The icing weights in Table 1 were recorded as 17.33g and 17.68g. For the composite nanopores in Figure 9d, the surface is also completely covered by ice, but the thinner ice layer is of a lower icing weight (14.83 g). After comparison, the contact of water droplets on the surface of the composite nanopore could be small. Raindrops could completely soak the surface at a fast rate and flow quickly along the wet surface to the lower edge of the sample to detach from the surface or form hanging icicles. Compared with the other three samples, the modified composite nanopore surface has a very small

amount of icing residue in Figure 9e and a low icing weight of 0.1 g in Table 1 due to its good water repellency, droplet motion behavior, and ice adhesion. When the raindrops make contact with the surface, droplets can easily roll or bounce off and hardly adhere to the surface. Moreover, under the action of gravity and raindrop impacts, the ice can easily break away from the surface due to the low ice adhesion strength, finally resulting in minor icing on the surface and a significant decrease in ice weight. Therefore, anodized specimens of composite nanopore structures can exhibit good anti-icing performance and have potential application prospects.

Table 1. Ice weight of different types of aluminum surfaces after 8 h of glaze icing.

Specimens	Substrate	Substrate (Modified)	Composite Nanopores	Composite Nanopores (Modified)
Icing weight (g)	17.33	17.68	14.83	0.10

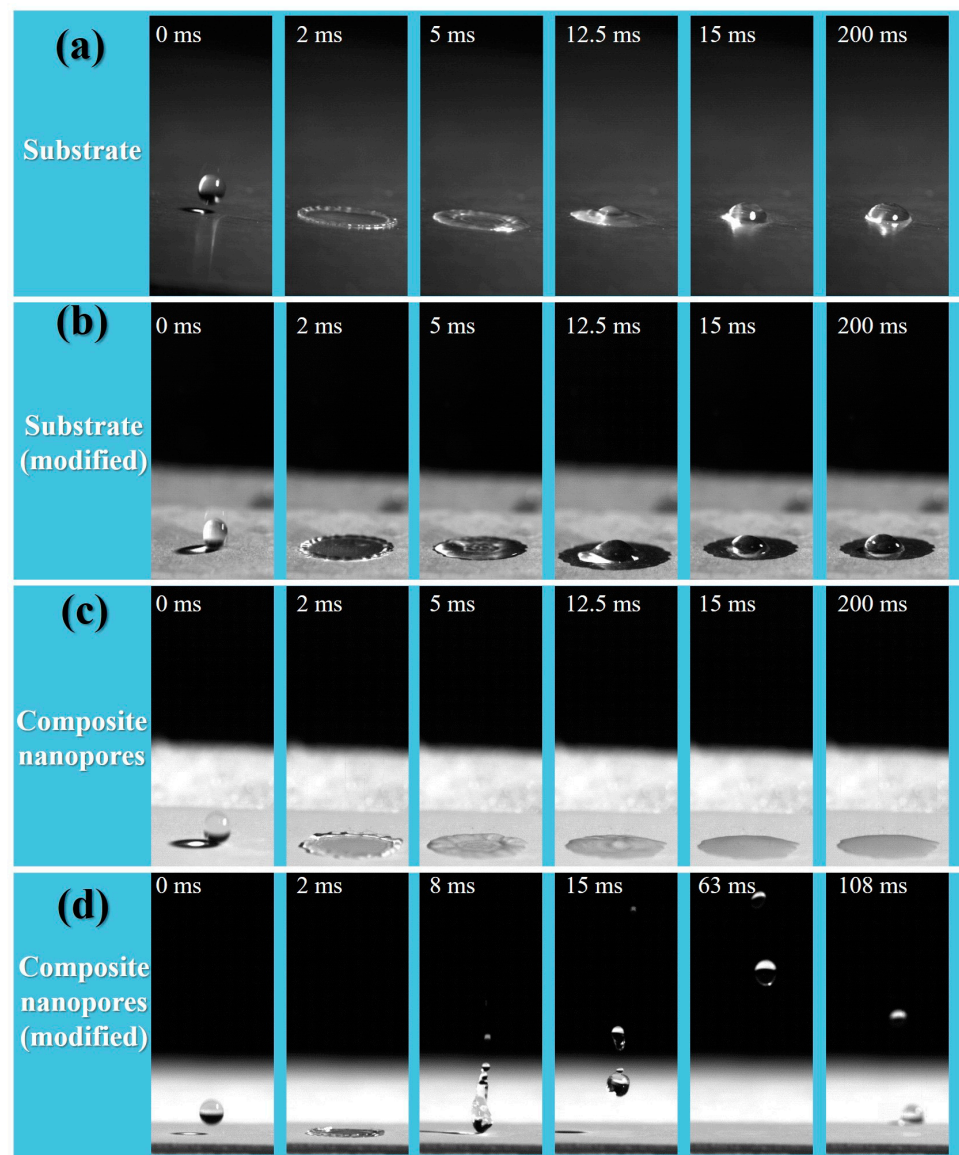


Figure 8. Motion behavior data of specimens before and after frosting: (a) substrate; (b) substrate (modified); (c) composite nanopores; (d) composite nanopores (modified).

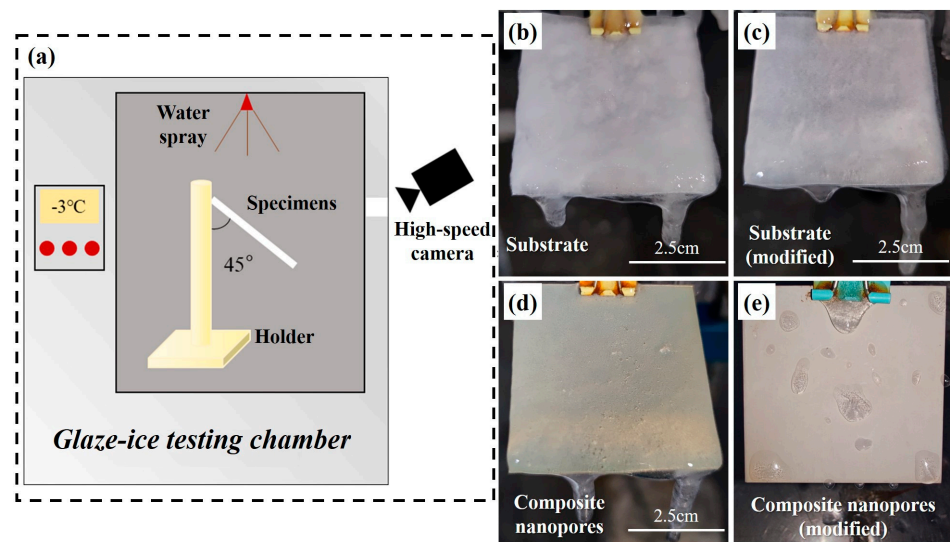


Figure 9. Glaze ice tests of different Al specimens: (a) glaze icing tests; (b) substrate; (c) substrate (modified); (d) composite nanopores; (e) composite nanopores (modified).

In all, for the prepared composite nanopore structure, the first step of phosphoric acid anodization has a significant impact on the upper nanopore's structure. The parameter settings refer to previous research to obtain appropriate porosity and roughness to achieve good anti-icing behavior [1]. Here, the concave defects of the thin barrier layer at the bottom of the nanopores were formed by the first anodization of phosphoric acid [15,16]. The second anodization of oxalic acid will start to dissolve from these defects and continue to passivate to form narrower nanopores in the lower layer [10,14,20]. Besides the effects of the etching and passivation, the second oxidation of oxalic acid will also have a dissolution effect on the upper nanopores formed under phosphoric acid anodization [10]. When the current density and oxidation time of the second anodization are increased, the roughness and fluctuation of the upper layer further increase, as shown in Figure 2. Therefore, the second step of the anodization process not only forms the lower layer nanopore's structure, but also has a dissolution effect on the upper layer nanopore's structure. Finally, by comparing the hydrophobicity and anti-icing performance, the optimal parameters for the second anodization to prepare composite pore structures were determined.

In particular, transmission lines with a special cylindrical geometry can significantly affect the fabrication of the composite nanopore structure [21]. In our previous studies, it was difficult to completely repeatedly prepare this nanopore structure with a similar geometric feature on the Aluminum Conductor Steel Reinforced (ACSR) cable as that of a flat Al substrate. For difficulties in the micro-structure formation on the cylindrical structure of the Al conductors, the processed area of the Al conductor needs to be considered to determine the electrical parameters of the anodization (current, voltage, time, etc.). In addition, a uniform electric field needs to be provided to prepare a uniform pore structure [21]. Otherwise, it will lead to inconsistent current flowing through the different areas on the ACSR surface, resulting in an uneven distribution of the nanopore structures at different positions, greater fluctuations, and provoking a susceptibility to concentrated heating leading to structural damage. After that, a closely similar micro-structure can be obtained on Al conductors, achieving hydrophobicity and anti-icing properties. However, the anti-icing behavior of the anodized ACSRs is still difficult to achieve that of the flat Al plates, which mainly reflected in gaps between strands of the ACSRs, causing the easy capture of water droplets and the failure of the Cassie hydrophobic state [10].

Moreover, similar to the precautions for the first anodization on Al overhead transmission lines, the second anodization needs to further consider the appropriate electrical parameters to form the composite nanopore structure with a similar geometric feature. Moreover, ultrasonic cleaning with deionized water should be considered between twice

anodization to ensure no phosphoric acid and impure residue remains on the surface of the Al conductors. Finally, superhydrophobic ACSRs with these composite nanopores could be fabricated.

In this study, the preparation and anti-icing properties of superhydrophobic composite nanopore structures were preliminarily explored on Al plates. For comparison, Table 2 provides widely reported studies on anti-icing superhydrophobic Al plates [1,10,17,22]. Obviously, the anodized Al plates with composite structures in this study show a low ice adhesion and delayed frosting time. Although an outdoor snow icing test was not performed [17], glaze icing tests show a significant improvement compared with previous studies from our group [1,10]. Therefore, a superhydrophobic Al surface with this composite nanopore shows profound application potential. Recently, our group has also reported this composite nanopore structure on SLIPS film. Nevertheless, the preparation and related properties of superhydrophobic ACSRs with this composite nanopore structure still need further studies in the future.

Table 2. Comparison in wettability and anti-icing properties of different superhydrophobic aluminum surfaces.

Specimens with Structures	Technique	Contact Angle (°)	Anti-Icing Behavior	Ref.
Anodized Al plate with composite structure	Anodization	172	0.79 kPa; delay frosting to 2 h; 0.1 g ice formed after 8 h of the glaze icing	This study
Acid-etched surface with FAS	Acid etching	165	0.58 kPa	[22]
Polyamide mesh structure with SiO ₂ nanoparticles	Depositing	153	1.9 kPa; delay frosting to ~18 min	[1]
Nano-texture by laser processing	Laser ablation	153	Little snow accumulated on the surface after outdoor time of 3 years	[17]
Anodized Al plate with single structure	Anodization	156	Some big glaze ice at the top edge after 80 min	[1]
Slippery surface with dendritic structure	Anodization and SLIPS	~105	~5 kPa; 1.9 g ice formed after 3 h of the glaze icing	[10]

4. Conclusions

In this study, a two-step anodizing method was used to successfully prepare a composite nanopore structure on Al conductors by adjusting the anodizing parameters (current density and anodized time). The microstructure, hydrophobicity, and anti-icing properties of the composite nanopore structure were compared and studied. Moreover, bare substrate and optimal anodized specimens with and without modifications were also compared and discussed in hydrophobicity and glaze icing behaviors. Detailed conclusions were as follows:

- (1) The optimal preparation process is to conduct secondary oxidation in oxalic acid electrolyte with an anodization current density of 0.04375 A/cm² and anodization time of 15 min. As the current density and time increase, the surface roughness and fluctuation of anodized samples increases with the thicker upper layer.
- (2) The composite nanopore Al surface of the optimal preparation parameter has excellent hydrophobic and anti-icing properties. Among these properties, the contact angle is 173°, the contact angle hysteresis is 0.122°, the ice adhesion strength is 0.71 kPa, and the icing weight after the 8 h glaze icing reaches 0.1 g.
- (3) In this study, a two-step anodizing method was used to prepare superhydrophobic Al surfaces with a composite nanopore structure which effectively improves the anti-icing performance of traditional anodized single nanopore structures, especially for glaze icing protection. This study can be helpful for the further preparation of this Aluminum Conductor Steel Reinforced (ACSR) cable. Moreover, the durability of anti-icing properties still needs further exploration.

Author Contributions: Conceptualization, X.D., C.Z. and Y.Y.; validation, B.L., J.B., L.Y., L.Z., T.Z., X.D., C.Z., X.H. and R.L.; formal analysis, B.L., J.B., L.Y., X.D., H.X. and R.L.; investigation, X.D., C.Z.; resources, B.L.; writing—original draft preparation, X.D.; writing—review and editing, X.D.;

visualization, B.L. and Y.Y. supervision, Y.Y. and R.L.; project administration, B.L.; funding acquisition, B.L. and Y.Y. All authors have read and agreed to the published version of the manuscript.

Funding: This research was funded by the Electric Power Research Institute of Guizhou Power Grid Co., Ltd., China (Contract No.0666002022030101HX00001).

Institutional Review Board Statement: Not applicable.

Informed Consent Statement: Not applicable.

Data Availability Statement: The raw/processed data required to reproduce these findings cannot be shared at this time due to legal or ethical reasons.

Conflicts of Interest: The authors declare no conflict of interest.

References

1. Li, B.; Bai, J.; He, J.; Ding, C.; Dai, X.; Ci, W.; Zhu, T.; Liao, R.; Yuan, Y. A Review on Superhydrophobic Surface with Anti-Icing Properties in Overhead Transmission Lines. *Coatings* **2023**, *13*, 301. [\[CrossRef\]](#)
2. Li, M.; Chen, T.; Guo, X.; Dong, L.; Chen, J.; Zhu, M. High flashover strength and superhydrophobic coatings by constructing porous surface structure. *High Volt.* **2023**, *8*, 728–738. [\[CrossRef\]](#)
3. Chengrong, L.; Yuzhen, L.; Xiang, C. Research issues for safe operation of power grid in China under ice-snow disasters. *Power Syst. Technol.* **2008**, *32*, 14.
4. Li, T.; Li, J. Analysis of icing accident in South China power grids in 2008 and its countermeasures. In Proceedings of the CIRED 2009—20th International Conference and Exhibition on Electricity Distribution—Part 1, Prague, Czech Republic, 8–11 June 2009; pp. 1–4.
5. Wang, J.; Fu, C.; Chen, Y.; Rao, H.; Xu, S.; Yu, T.; Li, L. Research and application of DC de-icing technology in china southern power grid. *IEEE Trans. Power Deliv.* **2012**, *27*, 1234–1242. [\[CrossRef\]](#)
6. Ji, K.; Rui, X.; Li, L.; Leblond, A.; McClure, G. A novel ice-shedding model for overhead power line conductors with the consideration of adhesive/cohesive forces. *Comput. Struct.* **2015**, *157*, 153–164. [\[CrossRef\]](#)
7. Dai, X.; Wu, L.; Ci, W.; Yao, W.; Yuan, Y.; Xie, Z.; Jiang, B.; Wang, J.; Andrej, A.; Pan, F. Dual self-healing effects of salicylate intercalated MgAlY-LDHs film in-situ grown on the micro-arc oxidation coating on AZ31 alloys. *Corros. Sci.* **2023**, *220*, 111285. [\[CrossRef\]](#)
8. Ci, W.; Chen, X.; Sun, Y.; Dai, X.; Zhu, G.; Zhao, D.; Pan, F. Effect of Zn on mechanical and corrosion properties of Mg-Sc-Zn alloys. *J. Mater. Sci. Technol.* **2023**, *158*, 31–42. [\[CrossRef\]](#)
9. Golovin, K.; Kobaku, S.P.R.; Lee, D.H.; DiLoreto, E.T.; Mabry, J.M.; Tuteja, A. Designing durable icephobic surfaces. *Sci. Adv.* **2016**, *2*, e1501496. [\[CrossRef\]](#)
10. Xiang, H.; Yuan, Y.; Zhu, T.; Dai, X.; Zhang, C.; Gai, Y.; Liao, R. A novel durable anti-icing slippery surfaces with dendritic porous structure. *Mater. Today Phys.* **2023**, *35*, 101137. [\[CrossRef\]](#)
11. Irajizad, P.; Nazifi, S.; Ghasemi, H. Icephobic surfaces: Definition and figures of merit. *Adv. Colloid Interface Sci.* **2019**, *269*, 203–218. [\[CrossRef\]](#)
12. Xiang, H.; Yuan, Y.; Zhu, T.; Dai, X.; Zhang, C.; Gai, Y.; Liao, R. Anti-Icing Mechanism for a Novel Slippery Aluminum Stranded Conductor. *ACS Appl. Mater. Interfaces* **2023**, *15*, 34215–34229. [\[CrossRef\]](#)
13. Lee, J.; Lee, M.-H.; Choi, C.-H. Design of Robust Lubricant-Infused Surfaces for Anti-Corrosion. *ACS Appl. Mater. Interfaces* **2022**, *14*, 2411–2423. [\[CrossRef\]](#) [\[PubMed\]](#)
14. Qin, Y.; Li, Y.; Zhang, D.; Xu, N.; Zhu, X. Wettability, durability and corrosion properties of slippery laser-textured aluminum alloy surface under water impact. *Surf. Coat. Technol.* **2020**, *394*, 125856. [\[CrossRef\]](#)
15. Liu, C.-Y.; Biring, S. Nanoplatfrom based on ideally ordered arrays of short straight and long beer bottle-shaped nanochannels. *Microporous Mesoporous Mater.* **2019**, *287*, 71–76. [\[CrossRef\]](#)
16. Lee, W.; Ji, R.; Gösele, U.; Nielsch, K. Fast fabrication of long-range ordered porous alumina membranes by hard anodization. *Nat. Mater.* **2006**, *5*, 741–747. [\[CrossRef\]](#) [\[PubMed\]](#)
17. Boinovich, L.B.; Emelyanenko, A.M.; Emelyanenko, K.A.; Modin, E.B. Modus Operandi of Protective and Anti-icing Mechanisms Underlying the Design of Longstanding Outdoor Icephobic Coatings. *ACS Nano* **2019**, *13*, 4335–4346. [\[CrossRef\]](#) [\[PubMed\]](#)
18. Parin, R.; Martucci, A.; Sturaro, M.; Bortolin, S.; Bersani, M.; Carraro, F.; Del Col, D. Nano-structured aluminum surfaces for dropwise condensation. *Surf. Coat. Technol.* **2018**, *348*, 1–12. [\[CrossRef\]](#)
19. Sastry, S. Ins and outs of ice nucleation. *Nature* **2005**, *438*, 746–747. [\[CrossRef\]](#)
20. Papadopoulos, C.; Rakitin, A.; Li, J.; Vedenev, A.S.; Xu, J.M. Electronic Transport in Y-Junction Carbon Nanotubes. *Phys. Rev. Lett.* **2000**, *85*, 3476–3479. [\[CrossRef\]](#)

21. Dai, X.; Yuan, Y.; Liao, R.; Liu, G.; Zhang, C.; Huang, H. Experimental Studies of a Novel Anti-Icing Aluminum Conductor With Excellent Durability and Improved Electrical Performance. *IEEE Trans. Power Deliv.* **2023**, 1–12. [[CrossRef](#)]
22. Wang, F.; Lv, F.; Liu, Y.; Li, C.; Lv, Y. Ice adhesion on different microstructure superhydrophobic aluminum surfaces. *J. Adhes. Sci. Technol.* **2013**, *27*, 58–67. [[CrossRef](#)]

Disclaimer/Publisher’s Note: The statements, opinions and data contained in all publications are solely those of the individual author(s) and contributor(s) and not of MDPI and/or the editor(s). MDPI and/or the editor(s) disclaim responsibility for any injury to people or property resulting from any ideas, methods, instructions or products referred to in the content.